

## Article

# Analysis of Mixed Convection on Two-Phase Nanofluid Flow Past a Vertical Plate in Brinkman-Extended Darcy Porous Medium with Nield Conditions

Hatem Gasmi <sup>1,2</sup>, Umair Khan <sup>3,4</sup> , Aurang Zaib <sup>5</sup> , Anuar Ishak <sup>3</sup> , Sayed M. Eldin <sup>6</sup>  and Zehba Raizah <sup>7,\*</sup>

- <sup>1</sup> Department of Civil Engineering, College of Engineering, University of Ha'il, Hail 81451, Saudi Arabia  
<sup>2</sup> Laboratoire d'Ingénierie Géotechnique, Ecole Nationale d'Ingénieurs de Tunis, Université de Tunis El Manar, Tunis 1007, Tunisia  
<sup>3</sup> Department of Mathematical Sciences, Faculty of Science and Technology, Universiti Kebangsaan Malaysia, UKM, Bangi 43600, Malaysia  
<sup>4</sup> Department of Mathematics and Social Sciences, Sukkur IBA University, Sukkur 65200, Pakistan  
<sup>5</sup> Department of Mathematical Sciences, Federal Urdu University of Arts, Science & Technology, Gulshan-e-Iqbal, Karachi 75300, Pakistan  
<sup>6</sup> Center of Research, Faculty of Engineering, Future University in Egypt, New Cairo 11835, Egypt  
<sup>7</sup> Department of Mathematics, College of Science, King Khalid University, Abha 62529, Saudi Arabia  
\* Correspondence: zaalrazh@kku.edu.sa



**Citation:** Gasmi, H.; Khan, U.; Zaib, A.; Ishak, A.; Eldin, S.M.; Raizah, Z. Analysis of Mixed Convection on Two-Phase Nanofluid Flow Past a Vertical Plate in Brinkman-Extended Darcy Porous Medium with Nield Conditions. *Mathematics* **2022**, *10*, 3918. <https://doi.org/10.3390/math10203918>

Academic Editor: Vasily Novozhilov

Received: 23 September 2022

Accepted: 20 October 2022

Published: 21 October 2022

**Publisher's Note:** MDPI stays neutral with regard to jurisdictional claims in published maps and institutional affiliations.



**Copyright:** © 2022 by the authors. Licensee MDPI, Basel, Switzerland. This article is an open access article distributed under the terms and conditions of the Creative Commons Attribution (CC BY) license (<https://creativecommons.org/licenses/by/4.0/>).

**Abstract:** The rapid advancement in technology in recent years has shown that nanofluids are very vital to further development in science and technology. Moreover, many industrial specifications cannot be met by allowing natural convection only, hence the need to incorporate forced convection and natural convection into a single flow regime. The research aims to quantify the mixed convective two-phase flow past a vertical permeable surface in a Brinkman-Extended Darcy porous medium (BEDPM) induced by nanofluid, with heat and mass transfer. In addition, the Nield condition is also incorporated. The model of the problem was initially constructed in the vital form of leading governing equations (LGEs). These LGEs are specifically called partial differential equations (PDEs) (because of two or more independent variables) which were later converted into a set of the single independent variable of ordinary differential equations (ODEs) by implementing the similarity transformations. The set of single independent ODEs was numerically solved via the boundary value problem of fourth-order (bvp4c) technique. The bvp4c is one of the most frequently recommended built-in MATLAB subroutines based on the three-stage Labatto formula. The impact of several physically embedded influential parameters on the fluid flow, along with mass and thermal properties of the nanofluid in a Brinkman-Extended Darcy porous medium for the cases of buoyancy assisting flow (BAF) and buoyancy opposing flow (BOF), were investigated and argued. The numerical outcomes clarify that the porosity parameter reduces the velocity, whereas the concentration and the temperature enhance in the case of the buoyancy assisting and buoyancy opposing flows. In addition, the wall drag force elevates for the larger value of the dimensionless permeability parameter  $K_1$  and the buoyancy ratio parameter  $N$ , while it declines for the modified porosity parameter  $\varepsilon_1$ .

**Keywords:** nanofluid; porous medium; buoyancy impact; Nield condition

**MSC:** 76D05; 76D10

## 1. Introduction

Heat transfer improvement in industrial and engineering applications has received a lot of interest from researchers in recent years. This is because the reliability of most equipment in several fields, such as heat exchangers and electronic devices, is highly dependent on the phenomenon of heat transport. Due to their very small thermal conductivity,

base fluids such as ethylene glycol, water, and oil limit the rate of heat transfer. The aforementioned fluids' deficiencies are overcome by incorporating a single kind of nano-sized particle into these fluids. Choi and Eastman [1] were the first to address this process and referred to the resulting mixture as a nanofluid. Researchers have considered a variety of nanoparticle combinations, including metal oxides ( $\text{Al}_2\text{O}_3$ ,  $\text{CuO}$ ), semiconductors ( $\text{SiO}_2$ ,  $\text{TiO}_2$ ), as well as metals ( $\text{Cu}$ ,  $\text{Fe}$ ,  $\text{Al}$ ). Therefore, distinct works on nanoparticles can be found in the books of Das et al. [2], Minkowycz et al. [3], and Minea [4] as well as recent research papers by Zaib et al. [5], Usman et al. [6], Waini et al. [7], Kotresh et al. [8], Khan et al. [9], Abderrahmane et al. [10–12].

In contrast, employing nanoliquid saturated in a porous media is a well-organized method to develop the characteristics of convection heat transfer for industrial processes. As a result, researchers have paid close attention to the porous media procedure. This is because in several engineering areas, including groundwater, oil flow filtration, thermal insulation, and entire types of heat exchangers, a similar type of scheme was encountered. It can also be found in combustion schemes, cooling of electronic equipment, and turbine blades cooling, where heating or cooling is needed. The mixing of high and low-energies fluids has a great impact on the ability of these devices. Merkin [13] investigated the mixed convective flow through a vertical plate embedded in a porous media and discovered that the presence of double solutions occurs in the opposing flow. Later, Ahmad and Pop [14] stretched this problem to nanofluid flow. The mixed convective flow through a horizontal circular cylinder induced by nanofluid saturated in a porous media was inspected by Nazar et al. [15]. They claimed that as the solid volume fraction increases, the magnitude of the friction factor decreases. Chamkha et al. [16] investigated the radiation impact on the fluid flow of mixed convective packed with a nanofluid past a wedge embedded in a porous medium. Roşca et al. [17] developed a mixed convective flow past a vertical flat plate through a porous medium filled with a nanofluid. According to their numerical results, the nanoparticle volume fraction reduces the velocity for the buoyancy assisting flow at the plate. Sheremet and Pop [18] investigated mixed convective flow within a square lid-driven cavity induced by a nanofluid, whereas Bakar et al. [19] scrutinized the radiation effect on the mixed convective flow through a nanofluid past a vertical permeable cylinder saturated in a porous medium, concluding that the nanoparticle of  $\text{Al}_2\text{O}_3$  travels quicker in separating the thicknesses of the boundary layer, followed by  $\text{Cu}$  and  $\text{TiO}_2$ . Waini et al. [20] found double solutions of mixed convective flow with hybrid nanofluid from a vertical flat surface immersed in a porous media.

Several realistic applications rely on heat and mass transfer, including food processing, automotive radiators, refrigeration, air conditioning, petrochemical refining, and microwave ovens. Dash and Das [21] examined the Hall current impact on magneto flow via a porous accelerated plate, along with the transfer of heat and mass characteristics induced by heat generation. The time-dependent free convective flow induced by rotating elastic viscous fluid past a porous vertical plate in a porous media with heat and mass transfer (HT and MT) is premeditated by Panda et al. [22]. Das et al. [23] explored the time-dependent flow with MT via a porous accelerated plate and obtained the solution numerically as well as analytically. Sanjayanand and Khan [24] examined the combined effects of heat and mass transfer on the flow induced by viscoelastic fluid past a stretched exponential sheet with viscous dissipation. The impact of mass transfer on the time-dependent flow past a stretchable sheet subjected to a porous medium and chemically reactive species was examined by Elbashbeshy et al. [25]. The agglomeration effects of mass and heat transfer on thin fluid film induced by nanofluid through a time-dependent stretchable sheet with a viscous dissipation effect were considered by Qasim et al. [26]. They observed that the heat transfer declines due to viscous dissipation as well as for nanofluids parameters. The exploration of Brownian motion on magneto flow of a Casson nanofluid from a stretchable sheet with irregular radiation was scrutinized by Ramudu et al. [27]. Recently, Alam and Marwat [28] inspected MT and HT in a viscous flow past an erratic permeable plate with irregular thickness.

The use of combined forced and natural convection is trending in industries and manufacturing sectors for heat and mass transmission in a fluid. The applications range from the installation of grain storage and electronic circuits to the extraction of oil and heat exchangers. In many of these applications, buoyancy forces are generated due to the diffusion of masses of different chemical species and pressure gradients at different spatial positions. The effect of buoyancy on heat and mass transfer is very significant and has been studied by many authors. Roşca et al. [29] analyzed the effects of buoyancy in a flow under a combined presence of forced and natural convection in a porous medium. The model is developed with the notion that the free stream velocity  $u_\infty$  is not equal to zero. A numerical analysis was conducted on the governing equations, and the results indicate a dual solution exists when the flow is opposing. Mahanthesh et al. [30] studied the effects of heat and mass transfer on natural convection flow. With the aid of Laplace transform, a closed-form solution was obtained for the proposed model. They found out that the flow and heat transfer can be controlled by adjusting the nanoparticle volume fraction. Waini et al. [31] administered the flow over a traveling needle-like surface and also established that the solution is non-unique for a certain range of values of the flow parameters. Similar results were observed, in that the two solution branches respond oppositely to the flow parameters. Meanwhile, Bakar et al. [32] administered the flow over a shrinking surface in the presence of slip factor and thermal radiation. Dual solutions were also observed and the results remained similar for the two solutions. The stability analysis shows that the lower branch is unstable while the branch of the upper solution is stable.

Based on a comprehensive assessment of the previously stated review of the literature, it is worth noting that no comprehensive exploration of nanofluid caused by mixed convection instabilities developed through a vertical plate subjected to a porous medium with infinite extensions under the Nield condition has been conducted. As a result of the numerous applications of nanofluids in modern nanotechnology and the cooling of sophisticated electronic and industrial equipment, this research not only provides the interactions of nanofluids over a vertical plate immersed in a Brinkman-extended Darcy porous medium, but also investigates the impact of Nield conditions on the transport phenomenon. The boundary layer equation is scaled down into the non-dimensional form by using some similarity transformation and the resulting non-dimensional equation is solved.

## 2. Mathematical Scenario of the Problem

Consider a steady flow near an impermeable vertical flat plate subject to mixed convection embedded in a porous medium filled with nanofluid flow flowing with non-uniform free-stream velocity  $u_\infty(x) = Ax$  and zero mass flux conditions. The analysis of HT and MT with the Brinkman-extended Darcy model was also incorporated in the given formulation, where we shall assume the velocity square term has been neglected. As portrayed in Figure 1, where the Cartesian coordinates  $x$  and  $y$  measured, respectively, along with the plate and normal to it. The plate is assumed to be kept at a constant temperature  $T_w$ , while  $T_\infty$  signifies the temperature of the surrounding fluid, where  $T_w > T_\infty$  corresponds to the heated plate (buoyancy assisting flow) while  $T_w < T_\infty$  corresponds to the cooling plate (buoyancy opposing flow). Moreover, the concentration  $C$  at a specific constituent on the fluid side of the plate varies from  $C_w$  to  $C_\infty$  in the solution through porous media with  $C_w > C_\infty$ . The following fundamental governing equations, which we can write down, were developed using the aforementioned conditions with the help of boundary-layer and Boussinesq approximations.

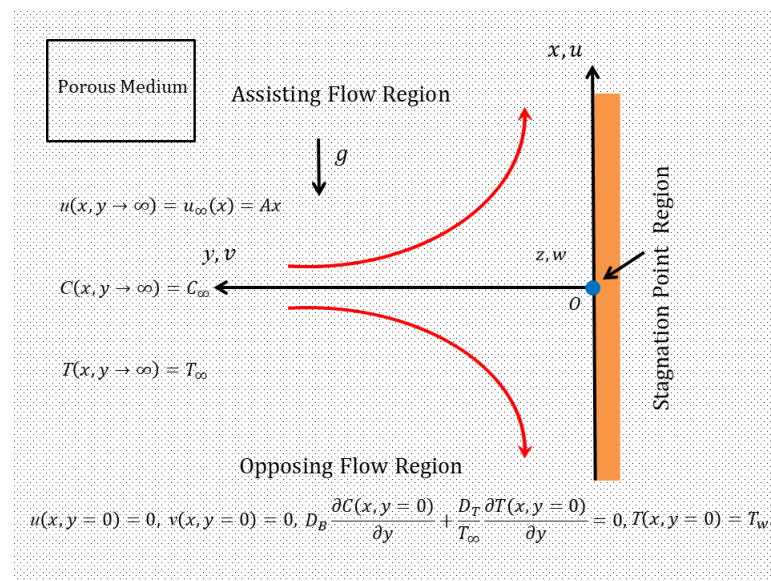


Figure 1. Physical model of the problem.

$$\frac{\partial u}{\partial x} + \frac{\partial v}{\partial y} = 0, \tag{1}$$

$$u \frac{\partial u}{\partial x} + v \frac{\partial u}{\partial y} = u_\infty \frac{du_\infty}{dx} + \epsilon^2 v_{eff} \frac{\partial^2 u}{\partial y^2} - \frac{\epsilon^2 v_f}{K} (u - u_\infty) + \epsilon^2 g \left[ \begin{matrix} (\beta_T)_f (T - T_\infty) \\ + (\beta_C)_f (C - C_\infty) \end{matrix} \right], \tag{2}$$

$$u \frac{\partial T}{\partial x} + v \frac{\partial T}{\partial y} - \tau \left[ D_B \frac{\partial T}{\partial y} \frac{\partial C}{\partial y} + \frac{D_T}{T_\infty} \left( \frac{\partial T}{\partial y} \right)^2 \right] = \alpha_f \frac{\partial^2 T}{\partial y^2}, \tag{3}$$

$$u \frac{\partial C}{\partial x} + v \frac{\partial C}{\partial y} - \frac{D_T}{T_\infty} \left( \frac{\partial^2 T}{\partial y^2} \right) = D_B \frac{\partial^2 C}{\partial y^2}. \tag{4}$$

For the current physical model, the subjected boundary conditions (BCs) are:

$$\begin{cases} u = 0, v = 0, T = T_w, D_B \frac{\partial C}{\partial y} + \frac{D_T}{T_\infty} \frac{\partial T}{\partial y} = 0, \text{ at } y = 0, \\ u \rightarrow u_\infty(x), T \rightarrow T_\infty, C \rightarrow C_\infty \text{ as } y \rightarrow \infty. \end{cases} \tag{5}$$

Here,  $(u, v)$  denote the components of velocity in  $(x-, y-)$  axes,  $T$  signifies the temperature,  $g$  signifies the acceleration because of gravity,  $\mu_f, \rho_f$  signify the dynamic viscosity and the density, respectively,  $\alpha_f$  thermal diffusivity,  $((\beta_T)_f, (\beta_C)_f)$  signify the corresponding coefficients of thermal and concentration volumetric expansions,  $(D_B, D_T)$  signify the coefficients of Brownian and the thermophoretic diffusions,  $\tau$  signifies the ratio of the effective heat capacity of the solid nanoparticles to the heat capacity of the working base fluid's and  $K$  signifies the permeability of the porous medium.

To further simplify the examination of the model, substantial similarity transformations are introduced [13]:

$$\eta = y \sqrt{\frac{u_\infty}{x \alpha_f}}, \psi = \sqrt{x u_\infty \alpha_f} F(\eta), G(\eta) = \frac{T - T_\infty}{T_w - T_\infty}, S(\eta) = \frac{C - C_\infty}{C_w - C_\infty}, \tag{6}$$

where  $\psi$  indicates the stream function, characterized by  $v = -\partial\psi/\partial x$  and  $u = \partial\psi/\partial y$ . Further, differentiating the stream function to get the following simplest form of the velocity component can take place as follows:

$$u = u_\infty F'(\eta) \text{ and } v = -\sqrt{\frac{u_\infty \alpha_f}{x}} (F - \eta F'). \tag{7}$$

For making the governing similarity equations, we have to assume the values of  $(\beta_T)_f$  and  $(\beta_C)_f$  in the form  $(\beta_T)_f = x(\beta_T)_f^*$  and  $(\beta_C)_f = x(\beta_C)_f^*$  (see Mohamed et al. [33]), where  $(\beta_T)_f^*$  and  $(\beta_C)_f^*$  are arbitrary constants. Therefore, the aforementioned Equation (6) implies two buoyancy or mixed convection parameters  $\lambda \cong \lambda_T$  and  $N\lambda \cong \lambda_C$ , respectively, defined as:

$$\lambda_T = \frac{\varepsilon^2 g(\beta_T)_f^* (T_w - T_\infty)}{A^2} = \frac{Ra_{xT}}{Pe_x^2} Pr \text{ and } \lambda_C = \frac{\varepsilon^2 g(\beta_C)_f^* (C_w - C_\infty)}{A^2} = \frac{Ra_{xC}}{Pe_x^2} Pr, \tag{8}$$

where  $Ra_{xT} = \frac{\varepsilon^2 g(\beta_T)_f (T_w - T_\infty) x^3}{v_{eff} \alpha_f}$  and  $Ra_{xC} = \frac{\varepsilon^2 g(\beta_C)_f (C_w - C_\infty) x^3}{v_{eff} \alpha_f}$  are the respective Rayleigh numbers,  $Pe_x = \frac{u_\infty x}{\alpha_f}$  is the Peclet number,  $Pr = \frac{v_{eff}}{\alpha_f}$  is the Prandtl number, and the buoyancy or mixed convection ratio factor,  $N$ , which clarifies the rivalry between the concentration and thermal mixed convective forces, is demarcated as;

$$N = \frac{(\beta_C)_f^* (C_w - C_\infty)}{(\beta_T)_f^* (T_w - T_\infty)}. \tag{9}$$

Furthermore, the choice of negative or positive selection of  $(\beta_C)_f^*$  (see Bejan and Khair, [34]) suggests that the buoyancy ratio parameter will be negative or positive (see Equation (9)). On the other hand, the extraordinary condition  $\lambda_C = N\lambda$  excludes the character of the term mixed convective ratio constraint from the set of governing non-dimensional equations. Consequently, we examine the current model further by focusing solely on the rest of the comprised influential parameters. Hence, by substituting Equation (6) into the governing equations, we obtain:

$$\varepsilon_1 F''' + FF'' - F'^2 + 1 - K_1(F' - 1) + (G + NS)\lambda_T = 0, \tag{10}$$

$$G'' + FG' + NbS'G' + NtG'^2 = 0, \tag{11}$$

$$S'' + LeFS' + \frac{Nt}{Nb}G'' = 0, \tag{12}$$

along with boundary conditions (BCs) are:

$$\begin{cases} F'(0) = 0, F(0) = 0, G(0) = 1, NbS'(0) + NtG'(0) = 0 \text{ at } \eta = 0, \\ F'(\eta) \rightarrow 1, G(\eta) \rightarrow 0, S(\eta) \rightarrow 0 \text{ as } \eta \rightarrow \infty. \end{cases} \tag{13}$$

In the above equations, the dimensionless control parameters are the Brownian diffusion parameter, the thermophoresis parameter, the modified porosity parameter, the dimensionless permeability parameter, and the Lewis number. These are defined in the mathematical notations as:

$$Nb = \tau(C_w - C_\infty)D_B/\alpha_f, Nt = \tau(T_w - T_\infty)D_T/\alpha_f T_\infty, \varepsilon_1 = \varepsilon^2 v_{eff}/\alpha_f = \varepsilon^2 Pr, K_1 = \varepsilon^2 v_f/KA, Le = \alpha_f/D_B.$$

### 2.1. Skin Friction Coefficient

The skin friction coefficients or friction factor is defined as follows:

$$\left( Pe_x^{1/2}/Pr \right) C_f = \frac{\mu_f \left( \frac{\partial u}{\partial y} \right)_{y=0}}{\rho_f u_\infty^2} = F''(0). \tag{14}$$

### 2.2. Heat Transfer

The heat transfer is demarcated as follows:

$$Pe_x^{-1/2}Nu_x = \frac{x \left( -k_f \frac{\partial T}{\partial y} \right)_{y=0}}{k_f(T_w - T_\infty)} = -G'(0), \tag{15}$$

where  $Pe_x = u_\infty x / \alpha_f$  corresponds to the Peclet number. It is appealing to observe that due to modified conditions such as  $NbS'(0) + NtG'(0) = 0$ , the expression of mass transfer identically takes place to zero specified by Kuznetsov and Nield [35].

### 3. Numerical Methodology and Validation of the Code

In the present research work, the governing equations for a steady flow with heat and mass transfer near an impermeable vertical flat plate comprising buoyancy impact saturated in a porous media occupied with a two-phase nanofluid flow model along with subjected non-uniform free-stream velocity and zero mass flux conditions are mathematically modeled. These modeled sets of PDEs were changed into (ordinary) similarity equations by implementing the similarity variables. Mathematically, the composed form of the set of differential Equations (10)–(12) along with appropriate BCs (13) was coupled and highly nonlinear, therefore, the solution in the closed explicit form of these ODEs was complicated to find. For this reason, it is possible to use a well-known numerical process to which we may quickly revert to its effective strategies for achieving the emphasized goals or aims. In terms of computation, the bvp4c (boundary value problem of fourth-order) finite-difference approach is one of the most suggested built-in codes available in MATLAB sub-routines (Shampine et al. [36]), which may be used successfully to offer fourth-order correct results in this phenomenon. Therefore, the given method can be used to solve first-order initial value problems. To continue our scheme, here, we present the new-fangled notations which can be read as follows:

$$F = E_1, F' = E_2, F'' = E_3, G = E_4, G' = E_5, S = E_6, S' = E_7. \tag{16}$$

The nonlinear first-order set of ODEs can be documented due to the assessment of these new mathematical notations in the acquired similarity equations, which can take place as:

$$\begin{pmatrix} E_1' \\ E_2' \\ E_3' \\ E_4' \\ E_5' \\ E_6' \\ E_7' \end{pmatrix} = \begin{pmatrix} E_2 \\ E_3 \\ \frac{(E_2^2 - E_1 E_3 - 1 + K_1(E_2 - 1) - \lambda_T(E_4 + N E_6))}{E_5} \\ -E_1 E_5 - Nb E_5 E_7 - Nt E_5^2 \\ E_7 \\ -Le E_1 E_7 - \frac{Nt}{Nb} E_5' \end{pmatrix}, \tag{17}$$

and to measure the aforementioned Equation (17) to be a single-point boundary value problem (IVP). Therefore, the subject ICs (known and unknown) are premeditated by:

$$\begin{cases} E_1(0) = 0, E_2(0) = 0, E_3(0) = A_1, E_4(0) = 1, \\ E_5(0) = -\frac{Nb}{Nt} E_7(0), E_6(0) = A_2, E_7(0) = -\frac{Nt}{Nb} E_5(0). \end{cases} \tag{18}$$

Additionally, the values of unknown arbitrary constants  $A_1$  and  $A_2$  are assumed to be simple for problems with a single solution. Moreover, the procedure of the scheme had been illustrated practically and graphically by Chu et al. [37] and Khan et al. [38], respectively, in a clear-cut way: that the practice of the code is constantly repeated until the far-field BCs are held at once:

$$\{E_2(\eta \rightarrow \infty) = 0, E_4(\eta \rightarrow \infty) = 0, E_6(\eta \rightarrow \infty) = 0. \tag{19}$$

The mesh selection and error process are bolstered in this case by the continuous solution of residual. The error tolerance was fixed to  $10^{-6}$ . Moreover, the edge of the boundary layer thickness  $\eta = \eta_{\max}$  is taken to be a fixed finite value of seven, which can hold the border ailments (13) asymptotically for the variations of the distinct parameters to maintain the necessary accuracy, while the mesh-size selection value has been adjusted between 0.001 and 0.1. Based on these observations, several numerical values of the skin friction coefficient for varying values of  $\varepsilon_1$  and  $\lambda_T$  when  $K_1 = 1.0$  (without the influence of the other comprised controlling parameters) are quantitatively compared with the available former work of Rosali et al. [39] and Khan et al. [40] as elucidated completely in Table 1. This tabular demonstration shows that the current outcomes and the comparative ones are in superb settlement, indicating that the results supplied by the bvp4c numerical approach are unquestionably real and accurate.

**Table 1.** Validations of  $C_f$  for varying values of  $\varepsilon_1$  and  $\lambda_T$  when  $K_1 = 1.0$  and the rest of the controlling parameters are absent.

$\varepsilon_1$	$\lambda_T$	$C_f$		
		Rosali et al. [39]	Khan et al. [40]	Present Results
0.1	−0.5	4.1508	4.1389	4.13883456
	1.0	6.4874	6.4864	6.48737453
	2.0	7.7611	7.7614	7.76132675
0.5	−0.5	1.8821	1.8838	1.88374657
	1.0	2.8597	2.8453	2.84523589
	2.0	3.3944	3.3944	3.39431567
0.7	−0.5	1.5967	1.6008	1.60073245
	1.0	2.4074	2.4124	2.41232897
	2.0	2.8514	2.8499	2.84984563
1.0	−0.5	1.3418	1.3488	1.34371245
	1.0	2.0050	2.0050	2.00501345
	2.0	2.3690	2.3620	2.36201965

#### 4. Analysis of Results

This fragment of the research work is divulged particularly to demonstrate the detailed description of the results in the form of distinct tables as well as several graphs. The acquired tabular form and graphical behavior of the outcomes were constructed in the requisite form of the dimensionless velocity  $F'(\eta)$ , the concentration distribution  $S(\eta)$ , the temperature distribution  $G(\eta)$ , the shear stress or friction factor coefficient  $C_f$ , and the heat transfer  $Nu_x$ , as clarified in Figures 2–13 as well as in Tables 2 and 3. For the computational simulations, we have fixed the range, such as ( $\eta < \eta_\infty = 7.0$ ), to develop the asymptotically converged behavior of the curves owing to growing values of the embedded control flow parameters such as  $\varepsilon_1$  (modified porosity parameter),  $\lambda_T$  (mixed convection parameter),  $K_1$  (dimensionless permeability parameter),  $Nt$  (thermophoresis parameter),  $Nb$  (Brownian motion parameter),  $Le$  (Lewis number), and  $N$  (buoyancy ratio parameter), whose default or fixed values are  $\varepsilon_1 = 0.5$ ,  $K_1 = 1.2$ ,  $Nt = 0.1$ ,  $Nb = 0.1$ ,  $Le = 10$ , and  $N = 0.5$ . Meanwhile, the mixed convection parameter  $\lambda_T$  value has been taken to be 3 and −3 for the corresponding buoyancy assisting and buoyancy opposing flows, respectively, where the Prandtl number is taken to be fixed, such as 6.2 for the considered working base fluid (water).

**Table 2.** Numerical values of shear stress  $C_f$  for several values of influential parameters.

$\epsilon_1$	$K_1$	$N$	Assisting Flow	Opposing Flow
0.25	0.75	0.50	6.1487376	−0.98035728
0.50			4.1754402	−0.75291722
0.75			3.3192327	−0.59739661
1.00			2.8170001	−0.47427638
0.50	0.75	0.50	4.1754402	−0.75291722
	0.80		4.1854688	−0.74086792
	0.85		4.1955118	−0.72308883
	0.90		4.2055694	−0.69391372
0.50	0.75	0.40	4.1623374	−0.76864007
		0.43	4.1662691	−0.76368910
		0.46	4.1702001	−0.75894785
		0.50	4.1754402	−0.75291722

**Table 3.** Numerical values of heat transfer  $Nu_x$  for several values of influential parameters.

$\epsilon_1$	$Nt$	$Nb$	$Le$	$K_1$	$N$	Assisting Flow	Opposing Flow
0.25						0.75434984	0.21760305
0.50	0.10	0.10	10	0.75	0.50	0.70714096	0.22880305
0.75						0.67674755	0.23700267
1.00						0.65425212	0.25756980
0.50	0.10					0.70714096	0.22880305
	0.30					0.65015345	0.23965033
	0.50	0.10	10	0.75	0.50	0.60002187	0.23109820
	0.70					0.55559080	0.21769050
0.50	0.10	0.10	10	0.75	0.50	0.70714096	0.22880305
		0.11				0.70681943	0.22631427
		0.12				0.70655117	0.22514745
		0.13				0.70632394	0.22402853
0.50	0.10	0.10	2.0			0.71776362	0.15705795
			4.0			0.71119458	0.18919402
			10.0	0.75	0.50	0.70714096	0.22880305
			15.0			0.70625285	0.24466209
0.5	0.1	0.1	10	0.75	0.5	0.71776362	0.22880305
				0.80		0.70697765	0.23609696
				0.85		0.70681868	0.24595134
				0.90		0.70666444	0.26005883
0.5	0.1	0.1	10	0.75	0.40	0.70643304	0.22295484
					0.43	0.70664563	0.22485683
					0.46	0.70685804	0.22662686
					0.50	0.70714096	0.22880305

The influence of the modified porosity parameter  $\epsilon_1$  on the dimensionless velocity,  $F'(\eta)$ , the temperature distribution,  $G(\eta)$ , and the concentration distribution,  $S(\eta)$ , for the buoyancy assisting and opposing flows against the pseudo-similarity variable  $\eta$  is schematically revealed in Figures 2–4, respectively. From Figure 2, it is seen that  $F'(\eta)$  solution curves shrinkages for the phenomenon of BOF as well as BAF owing to the escalating values of  $\epsilon_1$ . Furthermore, the momentum boundary layer thickness for the case of opposing flow is lower as compared to the phenomenon of the buoyancy assisting flow owing to the larger value of the modified porosity parameter  $\epsilon_1$ . Graphically, the gap in the outcome curves for the buoyancy assisting flow (BAF) is more relative to the case of the buoyancy opposing flow (BOF) when we boosted up the significant impacts of the modified porosity parameter. Physically, it is observed that the effective kinematic viscosity of the nanofluidic medium upsurges directly with the larger value of the modified porosity parameter; as a result, the velocity of the nanofluid and the thickness of the momentum boundary layer decelerate as we move forward against the pseudo-similarity variable. On the other hand, the profiles of temperature and concentration distributions are continuously enriched for both cases of BAF and BOF, due to the augmentation of modified porosity parameter  $\epsilon_1$ , as clarified amazingly in the image form (see Figures 3 and 4), respectively. Further, it is noted from the outcomes that the thickness of the concentration and thermal boundary layer (TBL) escalates with higher  $\epsilon_1$ . Meanwhile, the gap for the solutions of temperature in both cases of mixed convection parameter looks completely similar, whereas for the solutions of concentration the gap in curves of BAF is more relative to the BOF, since the resistance to the nanofluid flow elevates with superior consequences of the modified porosity parameter, which ultimately upgraded the solution domain possibility for concentration and temperature profiles.

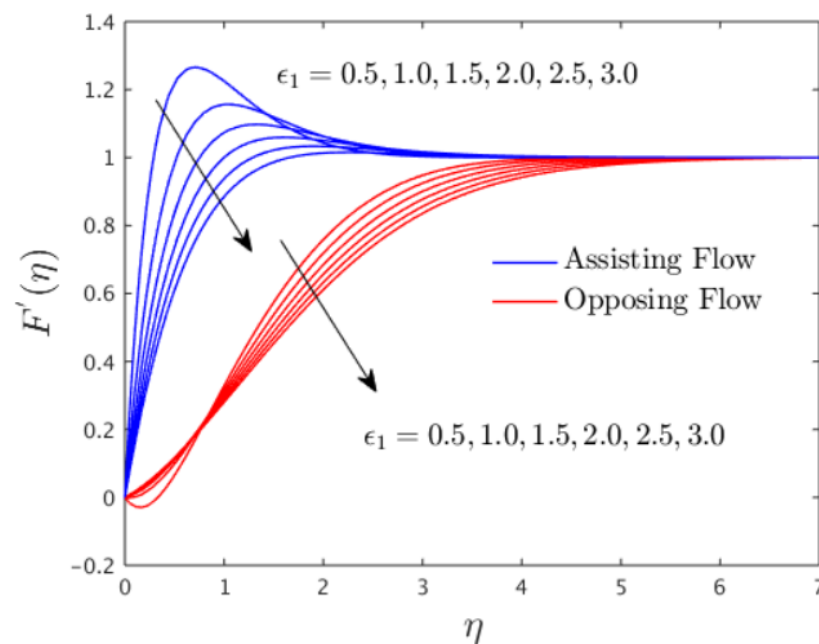


Figure 2.  $F'(\eta)$  against  $\epsilon_1$ .

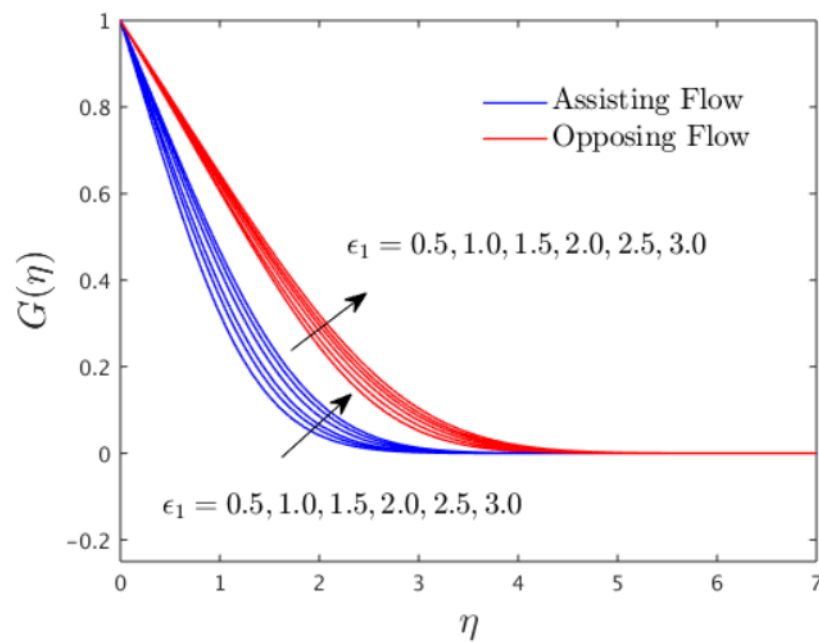


Figure 3.  $G(\eta)$  against  $\epsilon_1$ .

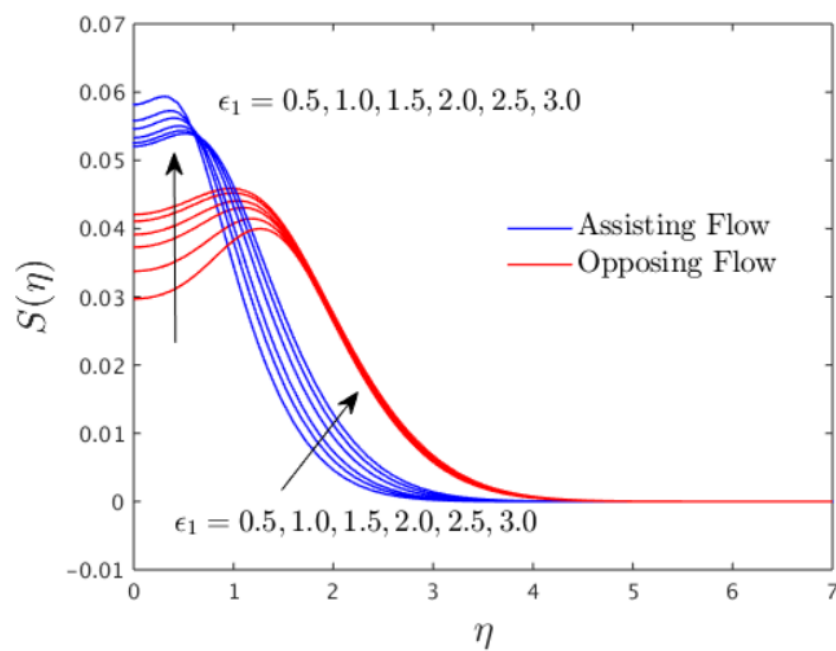


Figure 4.  $S(\eta)$  against  $\epsilon_1$ .

Figures 5–7 elucidate the influence of the dimensionless permeability parameter  $K_1$  on profiles of  $F'(\eta)$ ,  $G(\eta)$  and  $S(\eta)$  of the nanofluidic medium flow for the cases of BAF and BOF against the pseudo-similarity variable  $\eta$ , respectively. From the outcome of these images, it is detected that the velocity curves decline for BAF and incline for BOF due to the augmentation in the value of the permeability parameter while the behavior of the temperature and concentration distribution profiles are completely changed, and hence, ultimately, it is upsurges and shrinkages for both cases of BAF and BOF, respectively. In addition, the momentum BLT diminished but the thermal and concentration boundary layer elevates for the BAF due to the growing value of  $K_1$  while the entire profile tendency was opposite for the case of BOF owing to the augmentation in  $K_1$ . In general, a big dimensionless permeability parameter  $K_1$  is produced by a small permeability of a porous

medium  $K$ . Because the fluid may travel more freely due to the high permeability of a porous medium, a decrease in  $K_1$ , raises the velocity profile for the case of BAF. Since as velocity increases the temperature falls, and vice versa, as a result, as  $K_1$  decreases the temperature decreases. In addition, regarding the improving values of  $K_1$ , the gap between the solution curves of the concentration profiles for both cases of BAF and BOF are comparatively larger than the gap available in the solution curves of the temperature distribution and velocity profile.

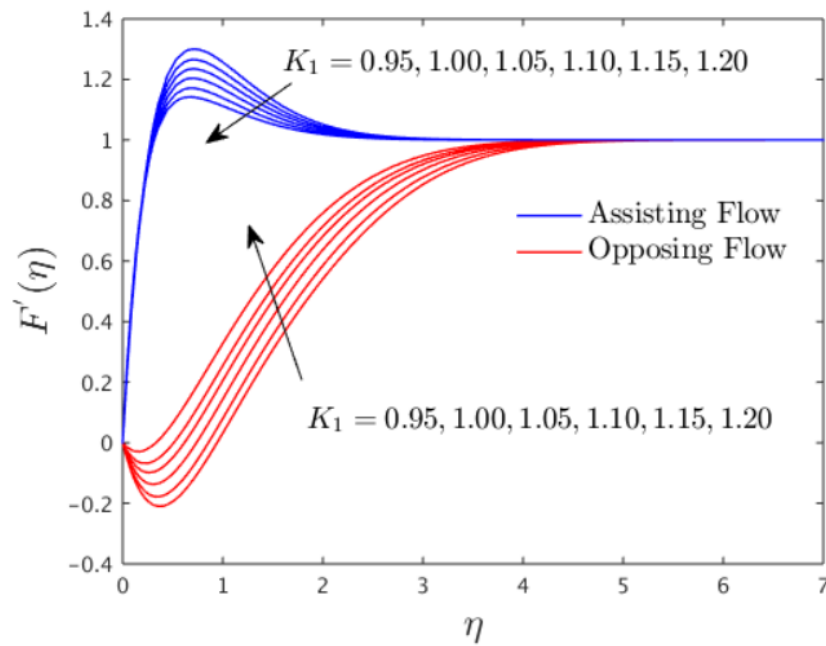


Figure 5.  $F'(\eta)$  against  $K_1$ .

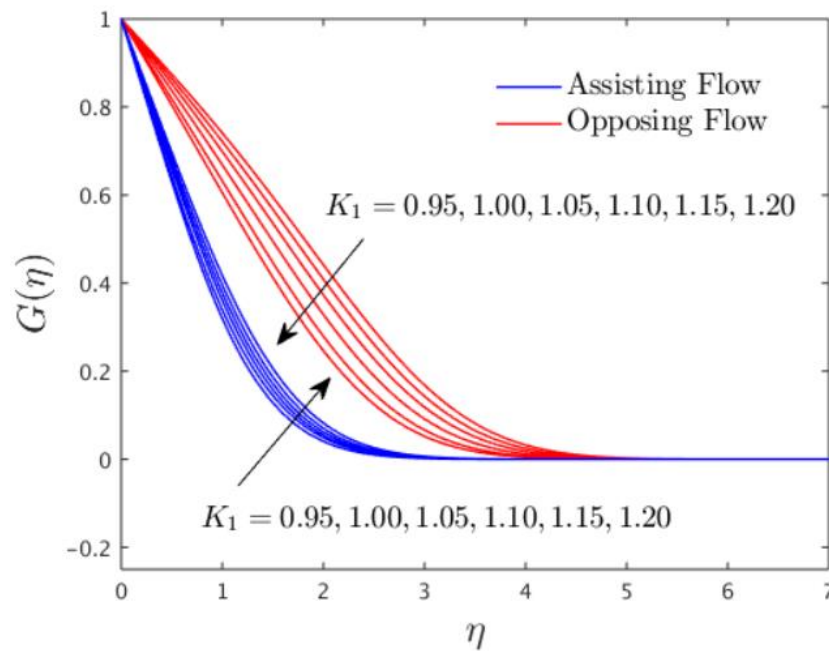


Figure 6.  $G(\eta)$  against  $K_1$ .

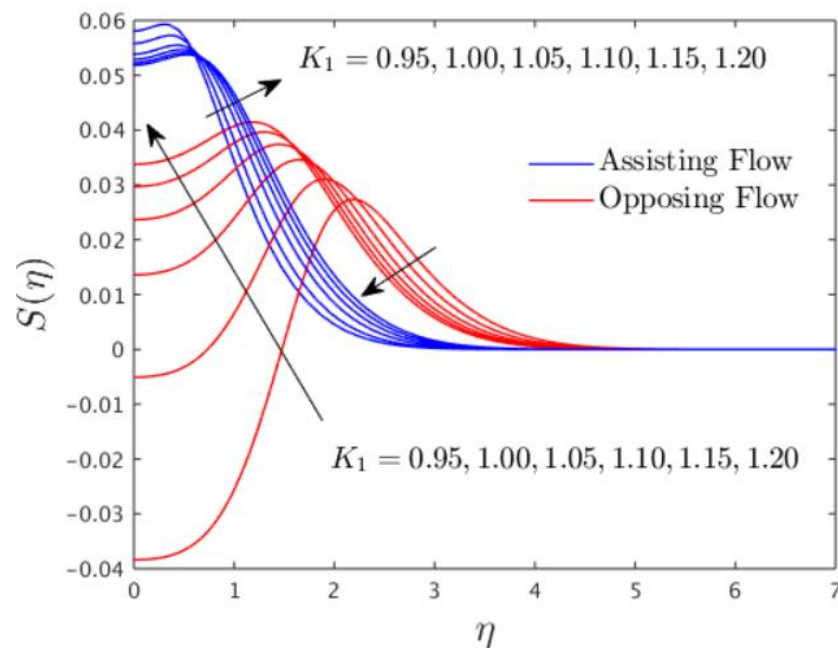


Figure 7.  $S(\eta)$  against  $K_1$ .

The consequence of the thermophoresis diffusion parameter  $Nt$  on the temperature distribution  $G(\eta)$  and concentration distribution  $S(\eta)$  for the cases of BAF and BOF are emphasized in Figures 8 and 9, respectively. From Figure 8, it seems to be worth mentioning that for both cases of buoyancy or mixed convection parameter, the ascending motion of nanomaterials helps to simplify heat transport filled with a nanofluidic medium by increasing  $G(\eta)$  and thickening the related region of the boundary layer. Alternatively, the concentration profile upsurges for the case of BAF due to the larger  $Nt$ , while for the case of BOF, the tendency of concentration solution curves initially declines and then is ultimately boosted (see Figure 9). In addition, the gap in the solution curves of the temperature profile is slightly lesser than the gap available in the concentration profile curves because of the enhancing value of the thermophoresis parameter  $Nt$ .

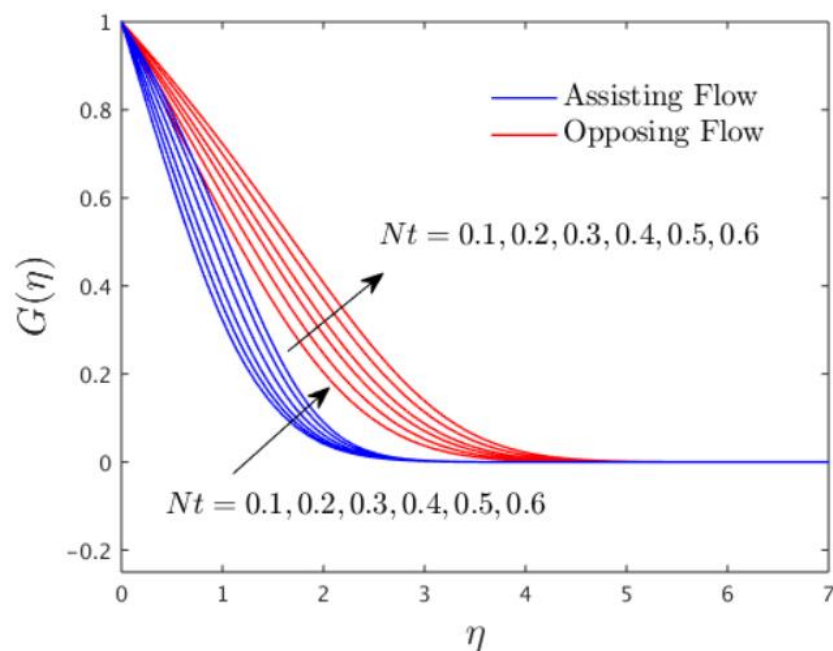


Figure 8.  $G(\eta)$  against  $Nt$ .

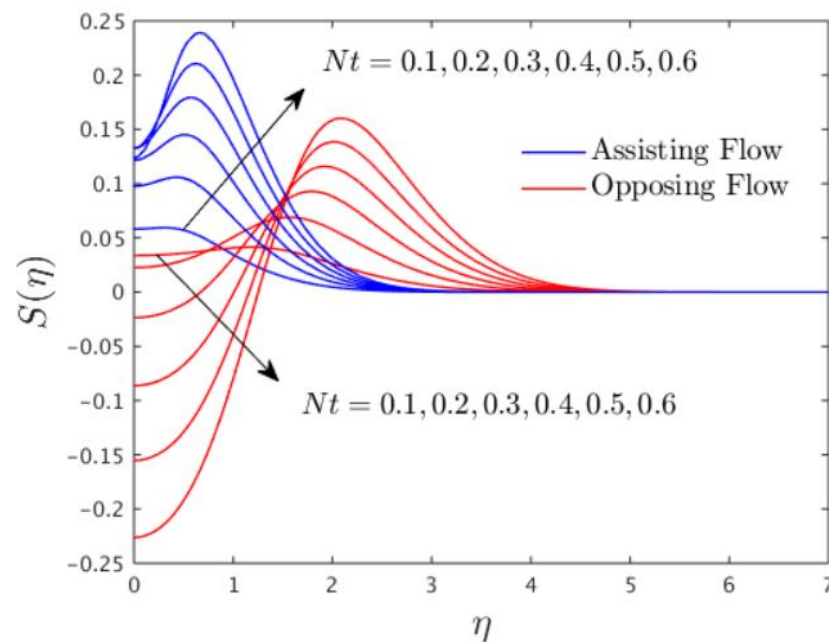


Figure 9.  $S(\eta)$  against  $Nt$ .

Figures 10 and 11 clarify the behavior of the temperature distribution  $G(\eta)$  and concentration distribution  $S(\eta)$  for the BAF and BOF, owing to the larger impacts of the Brownian motion parameter  $Nb$ , respectively. Outcomes reveal that the occurrence of Brownian mass diffusion term encourages the thermo-migration of fluid particles confines of a nanofluidic medium. Owing to this well-known statement, the temperature distribution  $G(\eta)$  elevates for the case of BAF and decelerates for BOF due to the escalating values of  $Nb$ , as emphasized in Figure 10. On the other hand, the concentration profile declines for the BAF and BOF if we increase the influences of  $Nb$ , as shown graphically in Figure 11. Further, this behavior of the outcomes was generally acceptable due to the superior values of  $Nb$ , which abruptly lessen the contribution of  $Nt$  in the concentration equation because of the diffusive term  $(Nt/Nb)(d^2S/d\eta^2)$ . Therefore,  $Nt$  and  $Nb$  divulge the opposite tendency towards  $\phi(\xi)$ .

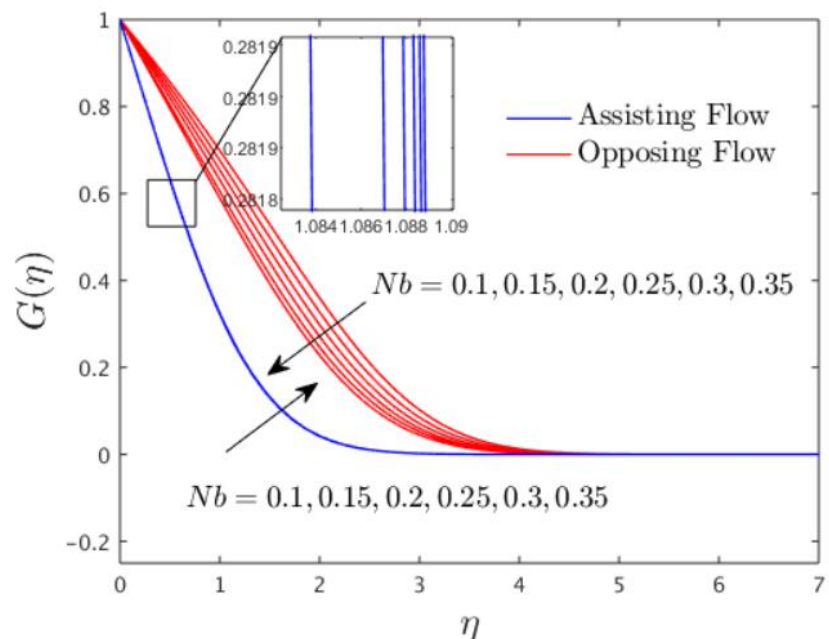
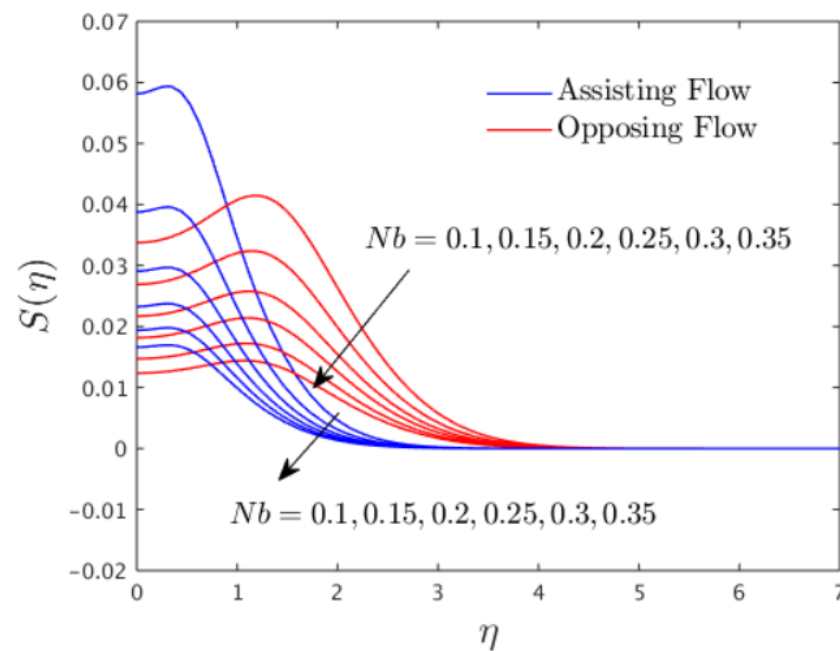


Figure 10.  $G(\eta)$  against  $Nb$ .



**Figure 11.**  $S(\eta)$  against  $Nb$ .

From an engineering perspective, the behavior of the outcomes of the shear stress  $C_f$  and heat transfer  $Nu_x$  for sundry values of the influential control parameters due to the cases of BAF and BOF are illustrated graphically and quantitatively in Figures 12 and 13 and Tables 2 and 3, respectively. Graphically, Figures 12 and 13 exemplify the influence of the modified porosity factor  $\varepsilon_1$  on the shear stress  $F''(0)$  and heat transfer  $-G'(0)$  profile for the BAF and BOF against the dimensionless permeability parameter  $K_1$ , respectively. Results demonstrate the shear stress  $F''(0)$  and heat transfer  $-G'(0)$  shrinkages for the case of BAF in the entire domain of  $K_1$ , escalating the modified porosity parameter  $\varepsilon_1$ , while for the case of BOF the  $F''(0)$  and  $-G'(0)$  initially grows and then declines for the rest of the domain against  $K_1$ . In the quantitative approach, Table 2 marks a significant improvement in shear stress  $C_f$  due to the boosted value of  $N$  (buoyancy ratio parameter), and  $K_1$  (dimensionless permeability parameter) for the cases of the buoyancy or mixed convection factor. At the same time, a diminishing behavior of the magnitude of friction factor is depicted for the case of BAF as well as BOF at the vertical plate surface of the porous medium owing to larger impacts of  $\varepsilon_1$  (modified porosity parameter). In the thermal properties, Table 3 reveals an improvement in the local Nusselt number  $Nu_x$  with the escalating value of the factors  $\varepsilon_1$  (modified porosity factor),  $Nt$  (thermophoresis diffusion parameter),  $Le$  (Lewis number),  $K_1$  (dimensionless permeability parameter), and  $N$  (buoyancy ratio parameter) for the case of BOF, while it is declined due to  $Nb$  (Brownian motion parameter). However, a weakening pattern was noticed in the heat transfer  $Nu_x$  for the larger support in the value of the constraints  $\varepsilon_1$  (modified porosity parameter),  $Nt$  (thermophoresis parameter),  $Nb$  (Brownian motion parameter),  $Le$  (Lewis number), and  $K_1$  (dimensionless permeability parameter) for the case of BOF, while it upsurges due to  $N$  (buoyancy ratio parameter).

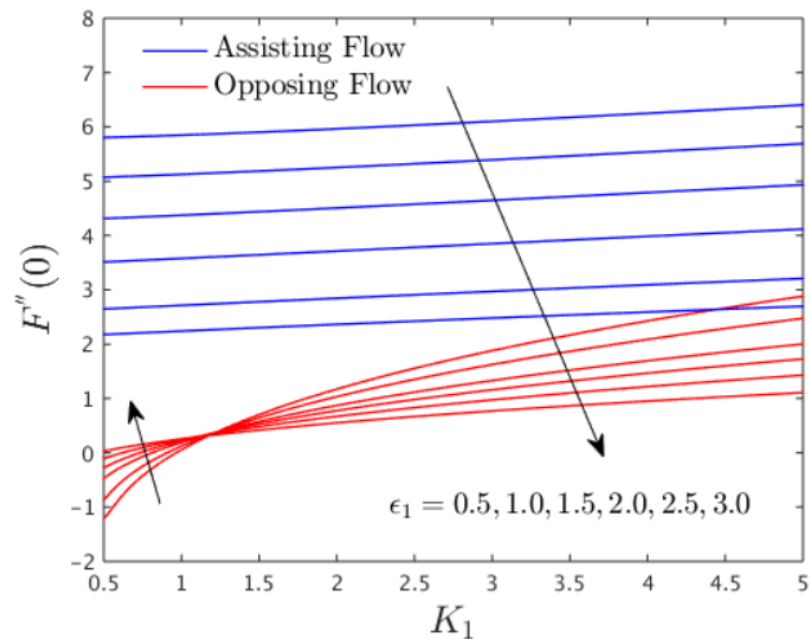


Figure 12. Variations of the shear stress for several values of  $\epsilon_1$ .

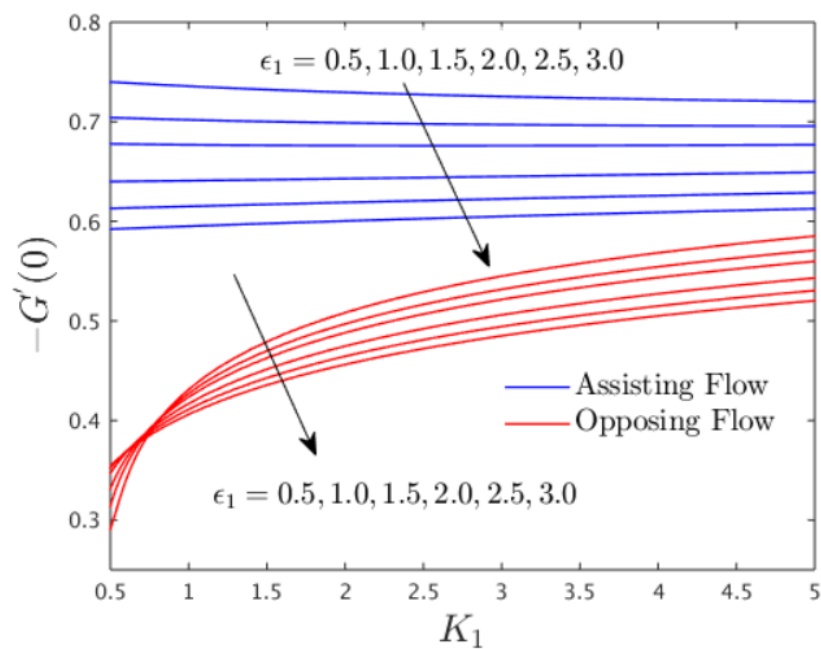


Figure 13. Variations of the heat transfer for several values of  $\epsilon_1$ .

### 5. Conclusions

The present research work was carried out to investigate the steady flow with heat and mass transfer near an impermeable vertical plate comprising the impact of mixed convection embedded in a porous media filled with a two-phase nanofluid flow model. The non-uniform free-stream velocity and Nield conditions are also incorporated in the current mathematical modeling of the problem. Therefore, the notable findings derived from the considered research work are as follows:

- Outcomes of the given model are discussed throughout the research work for the cases of buoyancy assisting flow (BAF) and buoyancy opposing flow (BOF) with several varying embedded control parameters.

- The profile of velocity declines for the case of BAF as well as BOF due to the larger impacts of  $\varepsilon_1$ , while the trend of velocity is the same for the case of BAF and the opposite for the case of BOF with the larger value of the dimensionless permeability parameter  $K_1$ .
- The dimensionless permeability parameter  $K_1$  and the Brownian motion parameter  $Nb$  raise the temperature for the case of BAF and decline for the case of BOF. On the other hand, the temperature abruptly improves for both cases of mixed convection parameter due to  $Nt$  and  $\varepsilon_1$ .
- The concentration profile decelerates for the case of BAF as well as BOF owing to higher impacts of parameter  $Nb$ , whilst the modified porosity parameter  $\varepsilon_1$  provides a substantial increment for both cases of buoyancy parameter.
- The local skin friction coefficient elevates for the larger value of  $K_1$  and  $N$  while it is declined for  $\varepsilon_1$ .
- The higher impacts of the buoyancy ratio parameter  $N$  enrich the wall mass transfer for the cases of BAF as well as for BOF.

It is worth mentioning that the work addressed above can be further extended by involving the time-dependent flow or involving some different aspects such as non-linear radiation, the application of solar energy, viscous dissipation, or chemical reaction. Moreover, the geometry has been changed from the vertical plate to a static wedge or cylinder.

**Author Contributions:** Conceptualization, U.K. and A.Z.; methodology, U.K. and A.Z.; software, U.K. and A.Z.; validation, U.K., H.G. and A.Z.; formal analysis, A.I., U.K., A.Z. and H.G.; investigation, A.I., Z.R. and S.M.E.; resources, Z.R.; data curation, A.I., H.G. and S.M.E.; writing—original draft preparation, A.I., H.G., S.M.E. and Z.R.; writing—review and editing, U.K., H.G., S.M.E. and Z.R.; visualization, Z.R.; supervision, A.I.; project administration, Z.R. and S.M.E.; funding acquisition, Z.R. and S.M.E. All authors have read and agreed to the published version of the manuscript.

**Funding:** This work was funded by the research center of the Future University in Egypt, 2022.

**Data Availability Statement:** Not applicable.

**Acknowledgments:** The authors are thankful for the partially support of the research center of the Future University in Egypt, 2022.

**Conflicts of Interest:** The authors declare no conflict of interest.

## References

1. Choi, S.U.S.; Eastman, J.A. Enhancing Thermal Conductivity of Fluids with Nanoparticles. In Proceedings of the 1995 International Mechanical Engineering Congress and Exhibition, San Francisco, CA, USA, 12–17 November 1995.
2. Das, S.K.; Choi, S.U.S.; Yu, W.; Pradeep, T. *Nanofluids: Science and Technology*; Wiley-Interscience: Hoboken, NJ, USA, 2007.
3. Minkowycz, W.J.; Sparrow, E.M.; Abraham, J.P. *Nanoparticle Heat Transfer and Fluid Flow*; CRC Press: New York, NY, USA; Taylor & Francis Group: Abingdon, UK, 2013.
4. Minea, A.A. *Advances in New Heat Transfer Fluids: From Numerical to Experimental Techniques*; CRC Press: New York, NY, USA; Taylor & Francis Group: Abingdon, UK, 2017.
5. Zaib, A.; Haq, R.U.; Sheikholeslami, M.; Khan, U. Numerical analysis of effective Prandtl model on mixed convection flow of  $\gamma\text{Al}_2\text{O}_3\text{-H}_2\text{O}$  nanoliquids with micropolar liquid driven through wedge. *Phys. Scr.* **2020**, *95*, 035005. [[CrossRef](#)]
6. Usman, M.; Zubair, T.; Hamid, M.; Haq, R.U. Novel modification in wavelets method to analyze unsteady flow of nanofluid between two infinitely parallel plates. *Chin. J. Phys.* **2020**, *66*, 222–236. [[CrossRef](#)]
7. Waini, I.; Ishak, A.; Pop, I. Nanofluid flow on a shrinking cylinder with  $\text{Al}_2\text{O}_3$  nanoparticles. *Mathematics* **2021**, *9*, 1612. [[CrossRef](#)]
8. Kotresh, M.J.; Ramesh, G.K.; Shashikala, V.K.R.; Prasannakumara, B.C. Assessment of Arrhenius activation energy in stretched flow of nanofluid over a rotating disc. *Heat Transf.* **2021**, *50*, 2807–2828. [[CrossRef](#)]
9. Khan, U.; Zaib, A.; Bakar, S.A.; Ishak, A. Stagnation-point flow of a hybrid nanofluid over a non-isothermal stretching/shrinking sheet with characteristics of inertial and microstructure. *Case Stud. Therm. Eng.* **2021**, *26*, 101150. [[CrossRef](#)]
10. Abderrahmane, A.; Al-Khaleel, M.; Mourad, A.; Laidoudi, H.; Driss, Z.; Younis, O.; Guedri, K.; Marzouki, R. Natural convection within inversed T-shaped enclosure filled by nano-enhanced phase change material: Numerical investigation. *Nanomaterials* **2022**, *12*, 2917. [[CrossRef](#)]
11. Abderrahmane, A.; Qasem, N.A.A.; Mourad, A.; Al-Khaleel, M.; Said, Z.; Guedri, K.; Younis, O.; Marzouki, R. Enhancing the melting process of shell-and-tube PCM thermal energy storage unit using modified tube design. *Nanomaterials* **2022**, *12*, 3078. [[CrossRef](#)]

12. Abderrahmane, A.; Younis, O.; Al-Khaleel, M.; Laidoudi, H.; Akkurt, N.; Guedri, K.; Marzouki, R. 2D MHD mixed convection in a zigzag trapezoidal thermal energy storage system using NEPCM. *Nanomaterials* **2022**, *12*, 3270. [[CrossRef](#)]
13. Merkin, J.H. Mixed convection boundary layer flow on a vertical surface in a saturated porous medium. *J. Eng. Math.* **1980**, *14*, 301–313. [[CrossRef](#)]
14. Ahmad, S.; Pop, I. Mixed convection boundary layer flow from a vertical flat plate embedded in a porous medium filled with nanofluids. *Int. Commun. Heat Mass Transf.* **2010**, *37*, 987–991. [[CrossRef](#)]
15. Nazar, R.; Tham, L.; Pop, I.; Ingham, D.B. Mixed convection boundary layer flow from a horizontal circular cylinder embedded in a porous medium filled with a nanofluid. *Transp. Porous Media* **2011**, *86*, 517–536. [[CrossRef](#)]
16. Chamkha, A.J.; Abbasbandy, S.; Rashad, A.M.; Vajravelu, K. Radiation effects on mixed convection over a wedge embedded in a porous medium filled with a nanofluid. *Transp. Porous Media* **2012**, *91*, 261–279. [[CrossRef](#)]
17. Roşca, N.C.; Roşca, A.V.; Groşan, T.; Pop, I. Mixed convection boundary layer flow past a vertical flat plate embedded in a non-Darcy porous medium saturated by a nanofluid. *Int. J. Numer. Methods Heat Fluid Flow* **2014**, *24*, 970–987. [[CrossRef](#)]
18. Sheremet, M.A.; Pop, I. Mixed convection in a lid-driven square cavity filled by a nanofluid: Buongiorno’s mathematical model. *Appl. Math. Comput.* **2015**, *266*, 792–808. [[CrossRef](#)]
19. Bakar, S.A.; Arifin, N.M.; Md Ali, F.; Bachok, N.; Nazar, R.; Pop, I. A stability analysis on mixed convection boundary layer flow along a permeable vertical cylinder in a porous medium filled with a nanofluid and thermal radiation. *Appl. Sci.* **2018**, *8*, 483. [[CrossRef](#)]
20. Waini, I.; Ishak, A.; Groşan, T.; Pop, I. Mixed convection of a hybrid nanofluid flow along a vertical surface embedded in a porous medium. *Int. Comm. Heat Mass Transf.* **2020**, *114*, 104565. [[CrossRef](#)]
21. Dash, G.C.; Das, S.S. Hall effects on MHD flow along an accelerated porous flat plate with mass transfer and internal heat generation. *Math. Eng. Indust.* **1999**, *7*, 389–404.
22. Panda, J.P.; Dash, G.C.; Das, S.S. Unsteady free convective flow and mass transfer of a rotating elasto-viscous liquid through porous media past a vertical porous plate. *AMSE J. Mod. Meas. Cont. B* **2003**, *72*, 47–59.
23. Das, S.S.; Sahoo, S.K.; Dash, G.C. Numerical solution of mass transfer effects on unsteady flow past an accelerated vertical porous plate with suction. *Bull. Malays. Math. Sci. Soc.* **2006**, *29*, 33–42.
24. Sanjayanand, E.; Khan, S.K. On heat and mass transfer in a viscoelastic boundary layer flow over an exponentially stretching sheet. *Int. J. Therm. Sci.* **2006**, *45*, 819–828. [[CrossRef](#)]
25. Elbashbeshy, E.M.A.; Emam, T.G.; Abdel-Wahed, M.S. Mass transfer over unsteady stretching surface embedded in porous medium in the presence of variable chemical reaction and suction/injection. *Appl. Math. Sci.* **2011**, *5*, 557–571.
26. Qasim, M.; Khan, Z.H.; Lopez, R.J.; Khan, W.A. Heat and mass transfer in nanofluid thin film over an unsteady stretching sheet using Buongiorno’s model. *Eur. Phys. J. Plus* **2016**, *131*, 16. [[CrossRef](#)]
27. Ramudu, A.C.V.; Kumar, K.A.; Sugunamma, V.; Sandeep, N. Heat and mass transfer in MHD Casson nanofluid flow past a stretching sheet with thermophoresis and Brownian motion. *Heat Transf.* **2020**, *49*, 5020–5037. [[CrossRef](#)]
28. Alam, A.; Marwat, D.N.K. Heat and mass transfer on a stretching/ shrinking and porous sheet of variable thickness with suction and injection. *Proc. Inst. Mech. Eng. Part C J. Mech. Eng. Sci.* **2021**, *235*, 5297–5308. [[CrossRef](#)]
29. Roşca, A.V.; Roşca, N.C.; Pop, I. Mixed convection heat and mass from a vertical surface embedded in a porous medium. *Transp. Porous Media* **2015**, *109*, 279–295. [[CrossRef](#)]
30. Mahanthesh, B.; Gireesha, B.J.; Gorla, R.S.R. Heat and mass transfer effects on the mixed convective flow of chemically reacting nanofluid past a moving/stationary vertical plate. *Alex. Eng. J.* **2016**, *55*, 569–581. [[CrossRef](#)]
31. Waini, I.; Ishak, A.; Pop, I. Dufour and Soret effects on Al<sub>2</sub>O<sub>3</sub>-water nanofluid flow over a moving thin needle: Tiwari and Das model. *Int. J. Num. Meth. Heat Fluid Flow* **2020**, *31*, 766–782. [[CrossRef](#)]
32. Bakar, S.A.; Md Arifin, N.; Khashi’ie, N.S.; Bachok, N. Hybrid nanofluid flow over a permeable shrinking sheet embedded in a porous medium with radiation and slip impacts. *Mathematics* **2021**, *9*, 878. [[CrossRef](#)]
33. Mohamed, M.K.A.; Salleh, M.Z.; Ishak, A. Effects of viscous dissipation on mixed convection boundary layer flow past a vertical moving plate in a nanofluid. *J. Adv. Res. Fluid Mech. Therm. Sci.* **2020**, *69*, 1–18. [[CrossRef](#)]
34. Bejan, A.; Khair, K.R. Heat and mass transfer by natural convection in a porous medium. *Int. J. Heat Mass Transf.* **1985**, *28*, 909–918. [[CrossRef](#)]
35. Kuznetsov, A.V.; Nield, D.A. Natural convective boundary-layer flow of a nanofluid past a vertical plate. *Int. J. Therm. Sci.* **2010**, *49*, 243–247. [[CrossRef](#)]
36. Shampine, L.F.; Gladwell, I.; Thompson, S. *Solving ODEs with Matlab*; Cambridge University Press: Cambridge, UK, 2003.
37. Chu, Y.M.; Khan, U.; Shafiq, A.; Zaib, A. Numerical simulations of time-dependent micro-rotation blood flow induced by a curved moving surface through conduction of gold particles with non-uniform heat sink/source. *Arab. J. Sci. Eng.* **2021**, *46*, 2413–2427. [[CrossRef](#)]
38. Khan, U.; Zaib, A.; Ishak, A.; Abu Bakar, S.; Animasaun, I.L.; Yook, S.-J. Insights into the dynamics of blood conveying gold nanoparticles on a curved surface when suction, thermal radiation, and Lorentz force are significant: The case of Non-Newtonian Williamson fluid. *Math. Comput. Simul.* **2022**, *193*, 250–268. [[CrossRef](#)]
39. Rosali, H.; Ishak, A.; Pop, I. Mixed convection stagnation-point flow over a vertical plate with prescribed heat flux embedded in a porous medium: Brinkman-extended Darcy formulation. *Trans. Porous Media* **2011**, *90*, 709–719. [[CrossRef](#)]
40. Khan, U.; Zaib, A.; Khan, I.; Nisar, K.S.; Baleanu, D. Insights into the stability of mixed convective Darcy–Forchheimer flows of cross liquids from a vertical plate with consideration of the significant impact of velocity and thermal slip conditions. *Mathematics* **2020**, *8*, 31. [[CrossRef](#)]